Research Article

For reprint orders, please contact: reprints@futuremedicine.com

Nanomedicine

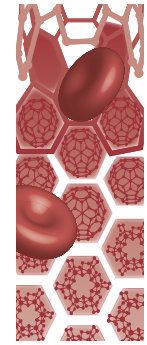

Neuronal commitment of human circulating multipotent cells by carbon nanotube-polymer scaffolds and biomimetic peptides

Aim: We aimed to set up a self-standing, biomimetic scaffold system able to induce and support *per se* neuronal differentiation of autologous multipotent cells. **Materials & methods:** We isolated a population of human circulating multipotent cells (hCMCs), and used carbon nanotube/polymer nanocomposite scaffolds to mimic electrical/nanotopographical features of the neural environment, and biomimetic peptides reproducing axon guidance cues from neural proteins. **Results:** hCMCs showed high degree of stemness and multidifferentiative potential; stimuli from the scaffolds and biomimetic peptides could induce and boost hCMC differentiation toward neuronal lineage despite the absence of exogenously added, specific growth factors. **Conclusion:** This work suggests the scaffold-peptides system combined with autologous hCMCs as a functional biomimetic, self-standing prototype for neural regenerative medicine applications.

First draft submitted: 8 April 2016; Accepted for publication: 16 May 2016; Published online: 1 June 2016

Keywords: biomimetic peptides • carbon nanotubes • human circulating multipotent cells • nanocomposite scaffold • neuronal differentiation • regenerative medicine

Giorgia Scapin[‡,§,1], Thomas Bertalot[‡,2], Nicola Vicentini[3], Teresa Gatti[3], Simone Tescari[2], Vincenzo De Filippis[2], Carla Marega[3], Enzo Menna[3], Marco Gasparella[4], Pier Paolo Parnigotto[5], Rosa Di Liddo*[,2] & Francesco Filippini**[,1]

[1]Department of Biology, University of Padua, 35131 Padua, Italy
[2]Department of Pharmaceutical & Pharmacological Sciences, University of Padua, 35131 Padua, Italy
[3]Department of Chemical Sciences, University of Padua, 35131 Padua, Italy
[4]Department of Woman & Child Health, University of Padua, 35128 Padua, Italy
5Tissue Engineering & Signaling ONLUS, Caselle di Selvazzano Dentro, 35030 Padua, Italy
*Author for correspondence:
Tel.: +39 049 827 5636
Fax: +39 049 827 5366
rosa.diliddo@unipd.it
**Author for correspondence:
Tel.: +39 049 827 6272
Fax: +39 049 827 6260
francesco.filippini@unipd.it
‡Authors contributed equally
§Present address: Section on Islet Cell & Regenerative Biology, Joslin Diabetes Center & Department of Medicine, Harvard Medical School, Boston, MA 02215, USA

Stem cells are central to cell and developmental biology as an invaluable tool for shedding light on mechanisms and events underlying cell and tissue differentiation; at the same time, multipotent cells can represent a precious autologous source for regenerative medicine. In the last two decades, bone marrow has been considered the main hematopoietic and multipotent stem cell source, but its clinical use faces some practical difficulties, such as a highly invasive extraction procedure, which is variable and dependent on the donors age [1]. For these reasons, alternative sources have been studied, such as umbilical cord, adipose tissue and peripheral blood [2–4]. Peripheral blood stem cell research represents an attractive option in the field of regenerative medicine as the clinical use of circulating stem cells is not limited by ethical restrictions or risks of immune rejection being derived from an autologous source. Most often, the stimulation of multipotent cells with specific growth factors is needed in order they are committed toward a specific cell lineage. However, a pivotal role in such commitment is also played by nanotopographical stimuli and guidance cues from the tissue environment. Thus, the combination of a self standing scaffold recapitulating such stimuli with autologous stem cells, which are highly responsive to biochemical and physical signals, can provide a front-end system helpful for regenerative medicine applications.

Nervous tissue is an intricate network of cells organized via multiple interactions with the extracellular environment that provides topographical and mechanical stimuli, bioactive molecule gradients and electrical signals. In particular, the commitment of progenitor cells toward neuronal lineage and

Future Medicine part of fsg

subsequent cell differentiation, neurite outgrowth and guidance are influenced by multiple factors: biochemical cues such as growth factors, cell adhesion molecules (CAMs) and extracellular matrix (ECM) proteins, which regulate cell proliferation and fate through the interaction with specific cell receptors; nanotopographical cues that are sensed by growth cones and guide neurite extension ensuring an appropriate connectivity within the overall neural circuitry; electrical cues that define the electroactive tissue while controlling neuronal cell growth and differentiation as well [5,6].

Therefore, in order to promote peripheral nerve regeneration and/or cell repopulation of central nervous system lesions, and finally to re-establish a functional neuronal network activity, scaffolds for neural regenerative medicine should recapitulate aforementioned regulatory cues to resemble native tissue environment features. Freestanding nanocomposite scaffolds combining the biocompatibility of poly-L-lactic acid (PLLA) matrix with the peculiar electrical, mechanical and chemical properties of carbon nanotubes (CNTs) [6–8] chemically functionalized and then dispersed at low concentration, proved functional in boosting neuronal differentiation of SH-SY5Y cells [9] (derived from human neuroblastoma) [10]. This could be further improved by electrospun scaffolds [11] with submicrometric fibers mimicking scale, 3D arrangement, nanoroughness and texture of the collagen and laminin fibrils of the neural ECM (ideal for cell adhesion and protein/growth factor retention) [12,13] as well as by the addition of synthetic peptides reproducing guidance motifs from CAM/ECM proteins involved in neurite outgrowth control [9].

However, while being neuroblastoma SH-SY5Y cells a robust and established cellular system for *in vitro* studies, human stem/multipotent cells are undoubtedly the best biological system to verify the suitability of scaffolds for regenerative medicine applications. Preliminary studies suggest that properly designed nanocomposite scaffolds may help in differentiation of neural stem precursors [14,15]; however, a freestanding scaffold able *per se* – in other words, even in the absence of classic growth factors – to commit autologous multipotent cells toward neuronal lineage, and to start neurite outgrowth and their neuronal differentiation, is not available yet.

This prompted us to isolate, characterize and use a population of human circulating multipotent cells (hCMCs) and to set up conditions by which biocompatible, nanocomposite scaffolds and biomimetic molecules [9,11] are able to drive such an autologous cell source toward neuronal lineage and early differentiation.

Materials & methods

Isolation of hCMCs

Circulating multipotent cells were isolated by Ficoll®Paque (Sigma-Aldrich, MO, USA) density gradient separation from human peripheral blood collected from healthy volunteer donors (n = 20; age: ≤12 years), under Italian ethic committee authorization and informed consent. Blood samples (5 ml) were diluted in α-Minimum Essential Medium (αMEM; Invitrogen Life Technologies, CA, USA; 1:1) and carefully layered onto Ficoll-Paque solution. After centrifugation (400 g for 20 min at 4°C), the upper layer was collected and resuspended in αMEM supplemented with 16.5% heat-inactivated fetal bovine serum (FBS; Invitrogen Life Technologies), 50 U/ml penicillin (Invitrogen Life Technologies), 50 µg/ml streptomycin (Invitrogen Life Technologies) and 1% L-glutamine (Sigma-Aldrich). Samples were seeded onto tissue culture plates and allowed to adhere for 24 h. Following a gentle washing in αMEM, cells were cultured in complete medium in humidified atmosphere of 5% CO_2 at 37°C. When fibroblast colony-forming cells (CFU-F) were detected, culture medium was changed and cell expansion was performed. At 80% confluence, hCMCs were detached using 0.02% EDTA/0.25% trypsin solution (Sigma-Aldrich) and subcultures were prepared with seeding density of 10^4 cells/cm^2.

Differentiation of hCMCs in culture

Cells cultured in αMEM (standard medium) were considered as untreated control. Cells were induced to differentiate by following culture conditions as described hereafter:

Adipogenic

hCMCs were seeded at a density of 10^4 cells/cm^2 and cultured in DMEM high glucose (Invitrogen Life Technologies), 10% FBS, 50 U/ml penicillin, 50 µg/ml streptomycin, 10 µg/ml insulin (Sigma-Aldrich), 0.5 mM isobutylmethylxanthine (Sigma-Aldrich), 1 µM dexamethasone (Sigma-Aldrich), 60 µM indomethacin (Sigma-Aldrich).

Osteogenic

hCMCs were seeded at 10^4 cells/cm^2 density and cultured in αMEM (Invitrogen Life Technologies), 10% FBS, 50 U/ml penicillin, 50 µg/ml streptomycin, 100 nM dexamethasone (Sigma-Aldrich), 10 mM β-glycerophosphate (Sigma-Aldrich), 50 µM ascorbic acid (Sigma-Aldrich).

Myogenic

hCMCs were seeded at 10^4 cells/cm^2 density and grown in standard medium before reaching of 90% conflu-

ence. Myogenic differentiation was obtained using a myogenic induction medium, composed of standard medium supplemented with 100 ng/ml IGF (Immuno-Tools GmbH, Friesoythe, Germany) and 200 µM ascorbic acid. The medium was changed every 3 days.

Neurogenic

hCMCs were seeded at 10^4 cells/cm^2 density in DMEM/F-12 (Invitrogen Life Technologies) supplemented with 16.5% FBS, 50 U/ml penicillin, 50 µg/ml streptomycin (day 0). After 24 h (day 1), the medium was replaced by DMEM/F-12 supplemented with 2% FBS (low FBS medium) and 10 µM retinoic acid (RA; Sigma-Aldrich) or dimethyl sulfoxide (Sigma-Aldrich) as equivalent amount (in which RA is dissolved).

Scaffold & peptide synthesis

The CNT–PLLA scaffolds were prepared as reported [9]. Briefly, commercially available multi-walled carbon nanotubes (MWCNTs; Sigma-Aldrich) were purified by two-steps treatment at high temperature, dispersion in aqueous HCl (37%), sonication and membrane filtration. MWCNTs were methoxyphenyl (PhOMe)-functionalized and dissolved with PLLA in chloroform under mild sonication. The resulting dispersion was drop-cast onto a glass dish to obtain the MWCNT-PhOMe@PLLA 0.25% scaffold (CNT–PLLA scaffolds). The electrospun-CNT–PLLA (eCNT–PLLA) scaffolds were prepared as reported [11]. Briefly, electrospinning was performed by passing a MWCNT-PhOMe@PLLA 0.25% solution through an 18G needle at a flow rate of 0.03 ml/min, applying an acceleration voltage of 18 kV between the needle and the collecting plane; the collector was electrically grounded at a working distance of 20 cm. Fibers were collected onto 13 mm diameter glass coverslips deposited onto a paper foil. The process was carried out at room temperature within a range of relative humidity (RH: 45–50%).

LINGO1-A (^{467}SAKSNGRLTVFPDG^{480}) and L1-A (^{178}HIKQDERVTMGQNG^{191}) peptides were synthesized and prepared as reported [9] by solid-phase method, purified to homogeneity (>98%) by reversed-phase high-performance liquid chromatography and characterized by high-resolution mass spectrometry.

Culture of hCMCs on nanocomposite scaffolds & LINGO1-A/L1-A peptides

In all experiments, cells were seeded at 12,000/well density in DMEM/F12 supplemented with 16.5% heat-inactivated FBS and 50 U/ml penicillin, 50 µg/ml streptomycin (culture medium). Twenty-four hours after cell seeding (day 1), the culture medium was replaced by the low FBS medium supplemented with 0.1% dimethyl sulfoxide. Round slices (13 mm diameter) of CNT–PLLA sheets or eCNT–PLLA fiber-covered coverslips were sterilized by UV irradiation and positioned into 24-well plates. Scaffolds were preincubated for 24 h in the culture medium prior to cell seeding. Forty-eight hours after cell seeding, peptides were added – except for control samples – at 1 µM concentration. Cells were maintained in culture for 5 days after cell seeding.

Scanning electron microscopy

Morphologic analysis was performed by scanning electron microscopy (SEM) on hCMCs seeded onto sterile glass slides and grown in αMEM medium. After 24 h, samples were fixed with 0.1 M cacodylate buffer solution, pH 7.2 (Sigma-Aldrich) in 3% glutaraldehyde (Sigma-Aldrich) and stored at 4°C until dehydration, performed by 3 × 5 min immersion steps in ethanol with increasing concentration (70%, 90%, 95%). Cells were then kept in absolute ethanol until analysis, and subsequently subjected to Critical Point Drying and metallized with gold. The images were acquired using a JSM 6490 scanning electron microscope (JEOL Inc., MA, USA).

Flow cytometry

The analysis of immunophenotipic properties was performed on short- and long-term cultures (corresponding to 4th and 40th passage, respectively) using primary antibodies reported in the scheme below. In parallel, controls were stained using only corresponding isotype and secondary antibodies (Table 1).

The positive expression of each target marker was assessed using the Overton subtraction tool of Summit 4.3 software (Beckman Coulter Inc., Brea, CA, USA). The expression of TUBβ3 was investigated by Flow cytometry (FCM) on hCMCs cultured in αMEM and DMEM/F-12 medium for 5 days on polystirene culture dishes or CNT–PLLA/eCNT–PLLA scaffolds and then treated with LINGO1-A or L1-A peptides. The analysis was performed using a mouse anti-human βIII Tubulin primary antibody (Merck Millipore) and a rabbit anti-mouse Alexa Fluor® 488 secondary antibody (Invitrogen Life Technologies). Cells cultured in standard medium were considered as reference. Data were acquired using a FACSCanto II Flow cytometer (BD Biosciences, CA, USA) and were reported as mean fluorescence intensity ± standard deviation (SD).

RNA extraction, reverse transcriptase-PCR & quantitative PCR

RNA from each sample was obtained after cell homogenization with TRIzol® reagent (Invitrogen Life Technologies), according to manufacturer's protocol. The

Table 1. Antibodies used for flow cytometry analysis.

Antibodies	Manufacturing company
Primary antibodies	
PE mouse anti-human CD14	Santa Cruz Biotecnology, Inc
FITC mouse anti-human CD33	BD Biosciences
PE-Cy7 mouse anti-human CD34	BD Biosciences
Mouse anti-human CD44	AbD Serotec
PE mouse anti-human CD45	Santa Cruz Biotecnology, Inc
PE mouse anti-human CD73	BD Biosciences
PE mouse anti-human CD90	Santa Cruz Biotecnology, Inc
PE mouse anti-human CD105	Santa Cruz Biotecnology, Inc
PE mouse anti-human HLA DR	Santa Cruz Biotecnology, Inc
Mouse anti-human Nestin	Merck Millipore
Secondary antibodies	
PE goat anti-mouse	Santa Cruz Biotecnology, Inc
Isotype controls	
PE isotype control	Santa Cruz Biotecnology, Inc
FITC isotype control	BD Biosciences
PE isotype control	BD Biosciences
PE-Cy7 isotype control	BD Biosciences

FITC: Fluorescein isothiocyanate; PE: Phycoerythrin; PE-Cy7: Phycoerythrin-cyanine7.

RNA was dried and dissolved in RNase-free water. RNA was quantified by measuring the absorbance at 260 nm with NanoDrop2000 (Thermo Fisher Scientific Inc., MA, USA).

One step reverse transcriptase-PCR

The expression of adipogenic, myogenic, osteogenic and neurotrophins genes was analyzed by reverse transcriptase-PCR (RT-PCR). Thirty nanogram of RNA were reverse transcribed and amplified using Qiagen One Step RT-PCR Kit (Qiagen, Hilden, Germany) and iCycler iQ™ (Bio-Rad Laboratories Inc., CA, USA). RT-PCR products were electrophoresed on a 2% agarose gel (Invitrogen Life Technologies) stained with GelRed™ (Biotium Inc., CA, USA) and visualized using a UV transilluminator Gel Doc 2000 Gel Documentation System (Bio-Rad Laboratories).

Quantitative PCR

The expression of pluripotent genes in undifferentiated hCMCs and neurogenic differentiation markers in all experimental groups was evaluated by quantitative PCR (qPCR). Reverse transcription was performed with GoScriptTM Reverse Transcription System and oligo(dT) primers (Promega Italia Srl, Milano, Italy) while the amplification reaction was carried out using Power SYBR® Green PCR Master Mix (Invitrogen Life Technologies) and a Rotor-Gene 3000 thermal cycler (Corbett Research, Sydney, Australia). At least three independent experiments were performed in triplicate; each qPCR experiment was performed for each sample in multiple technical replicates and each gene was run together with its own reference gene and a negative control. To assess the specific neurogenic commitment of hCMCs in all experimental conditions, the expression of non-neuronal genes was evaluated. The housekeeping controls for normalization were: *HPRT1* for pluripotent genes [16] and ribosomal protein *S13* for neuronal and non-neuronal genes [17]. The comparative CT method ($2^{-\Delta Ct}$) was used to quantify gene expression level. Primer pairs (from Invitrogen Life Technologies and Sigma-Aldrich) are reported below (F, Forward; R, Reverse) (Table 2).

Cell proliferation test

Resazurin reduction assay was performed as reported [9] to quantify metabolically active living cells and thus to monitor the effects of peptides and scaffolds on cell proliferation. The assay is based on the reduction of the indicator dye, resazurin (not fluorescent) to the highly fluorescent resorufin (Ex 569 nm, Em 590 nm) by viable cells. Nonviable cells rapidly lose their capacity to reduce resazurin and, thus, to emit fluorescent signals anymore. Briefly, the culture medium was replaced by

Table 2. Oligonucleotides used for the reverse transcriptase-PCR and quantitative PCR analysis

Genes	Primer sequences 5′-3′	Accession	Amplicon length
Pluripotent genes			
TERT	F: TCCGGAATGCCTCTGCTGTTATGA	NM_198253.2	63 bp
	R: ATGGACAAGCTGAGGAAGATG		
REX1	F: GAGATGGAGTAAGGAGGGAGAT	NM_174900.3	105 bp
	R: ATGGACAAGCTGAGGAAGATG		
SOX2	F: ATTCCAGAGAGACCTCTTTCATAAC	NM_003106.3	191 bp
	R: TACCTTTCTGCCCGTGAAGTGGAT		
STAT3	F: AAAGACAGCTACGTGGGTGACGAA	NM_213662.1	175 bp
	R: AGAACCTGCAGGAGGCAGAAGAAT		
NOTCH	F: AGGATCACACAGGTGGCCCATATT	NM_017617.3	112 bp
	R: AGCTAAAGCAGCAGCAAACTTCGG		
CMYC	F: ACATGAAGGAGCACCCGGATTACA	D10493.1	79 bp
	R: TGCGCTTCGCCTACAACTAGATCT		
Oct-4	F: TCGAGGAATTGCTCAAAGTGCTGG	NM_002701.4	102 bp
	R: ACACCAACGGCTGGAAGCTAAATC		
KLF4	F: GAAGATGCGCAGCAGCGAGAATTT	NM_004235.4	106 bp
	R: ACTTTCTCCTGTCCGTCATTGGCT		
NANOG	F: AGAATATGCACCAGGCCGAAGAGT	NM_024865.2	106 bp
	R: AGCTAAGAGTCTTTGGTGCTGGCT		
Neuronal genes			
Nestin	F: CAGGGGAGGACTAGGAAAAGA	NM_006617.1	257 bp
	R: GAGATGGAGCAGGCAAGAG		
TUBß3	F: AGGAAGAGGGCGAGATGTA	NM_006086.3	259 bp
	R: CAATAAGACAGAGACAGGAGCAG		
MAP2	F: ATAGACCTAAGCCATGTG	NM_002374.3	253 bp
	R: GGGACTGTGTAATGATCTC		
L1 CAM	F: CCCTGGAGAGTGACAACG	NM_000425.4	253 bp
	R: CCTGGACTCCACTATTCTAGGG		
SYP	F: TTTGTGAAGGTGCTGCAATGGGTC	NM_003179.2	337 bp
	R: TGGGCCCTTTGTTATTCTCTCGGT		
NGF	F: GCCCACTGGACTAAACTTCAGCA	NM_002506.2	356 bp
	R: GATGTCTGTGGCGGTGGTCTTA		
BDNF	F: GCAAACATCCGAGGACAAGGTG	NM_170735.5	244 bp
	R: GCTCCAAAGGCACTTGACTACT		
GDNF	F: GCGCTGAGCAGTGACTCAAATA	NM_000514.3	275 bp
	R: GTTTCATAGCCCAGACCCAAGT		
Non-neuronal genes			
LEP	F: CGGACAAGAGTTGGCTGTGCAAT	NM_000230.2	223 bp
	R: AGCTGGGTGGAAGAGAACACAGTT		
GBP	F: TCTTCTTGAGCTGGACCCACTGTT	X53698.1	238 bp
	R: ACCTCTAAGCCGAAGAAAGACTGC		

bp: Base pair; F: Forward; R: Reverse.

Table 2. Oligonucleotides used for the RT-PCR and quantitative PCR analysis (cont.).

Genes	Primer sequences 5′-3′	Accession	Amplicon length
Non-neuronal genes (cont.)			
TPM1	F: AAGCACATTGGTGAAGATGCCGAC	NM_001018005.1	244 bp
	R: TCAGCTTGTCGGAAAGGACCTTGA		
MYH7	F: AAGCTGCAGCAGTTCTTCAACCAC	NM_000257.3	254 bp
	R: GGTTGTCAAACAGCTTGGCCTTGA		
RUNX2	F: TCCGGAATGCCTCTGCTGTTATGA	NM_001024630.3	238 bp
	R: ACTGAGGCGGTCAGAGAACAAACT		
Reference genes			
S13	F: TACAAACTGGCCAAGAAGGG	NM_001017.2	259 bp
	R: GGTGAATCCGGCTCTCTATTAG		
HPRT1	F: ATGGACAGGACTGAACGTCTTGCT	NM_000194.2	79 bp
	R: TTGAGCACACAGAGGGCTACAATG		

bp: Base pair; F: Forward; R: Reverse.

500 µl of resazurin solution (Resazurin Sigma 15 µg/ml in growth medium without phenol red) and cells were incubated for 4 h in the dark at 37°C, 5% CO_2. Then, 200 µl of resazurin solution was removed twice from each well and transfered to a 96 well plate (technical duplicates). Fluorescence, directly correlated with cell quantity, was detected using a plate reader (Ascent Fluoroscan, excitation 540 nm, emission 590 nm). Background values from blank samples were subtracted and average values for the duplicates calculated. Cell proliferation was calculated from a calibration curve by linear regression using Microsoft Excel.

hCMCs morphological analysis

Control samples and hCMCs cultured on the scaffolds combined or not with peptides were stained with calcein acetoxymethyl ester (Calcein-AM; Biotium), a nonfluorescent cell permeable compound that when hydrolyzed by intracellular esterases in live cells converts to the strongly green fluorescent calcein (Ex 490 nm, Em 539 nm). This staining is particularly useful to visualize cells growing onto the scaffolds. Briefly, cells were incubated with 2 µM calcein-AM in Hank's Balanced Salt Solution (Invitrogen Life Technologies) for 30 min in dark at 37°C and 5% CO_2 and visualized under a DM4000b fluorescent microscope (Leica, Wetzlar, Germany) using GFP filter. Five images/well were recorded from five random fields (ten images for each condition), using a 20X objective. The first field was selected in the centre of the well. The next fields were selected in the four directions (north, south, west and east) from the first field. The morphological analysis was performed using LAS AF lite software (Leica) to define: no. of polarized cell/no. of cells, total protrusion length/no. of cells, no. of protrusions/no. of cells, total diameter length/no. of cells. The length of each neurite-like protrusion was measured from the cell body edge to the tip of the protrusion. Any protrusion shorter than half the cell body diameter was not considered as a neurite-like protrusion and therefore cells were not considered as polarized [18]. Cell diameter was measured as the longest distance between two edges in the cell body (major axis). Protrusion length and diameter were measured using LAS AF lite software (Leica).

Immunofluorescence

Five days after seeding, hCMCs were washed thrice with phosphate buffered saline (PBS; Euroclone Spa, Milano, Italy) and then fixed with BD Cytofix™ Fixation Buffer (BD Biosciences) for 20 min at 4°C. Permeabilization was performed using 0.2% Triton solution (Sigma-Aldrich) in PBS for 30 min at room temperature (RT) and non-specific sites were blocked with blocking solution (5% FBS in PBS) for 30 min at RT. hCMCs were then incubated with mouse MAB 1637 anti-neuron specific TUBβ3 (Merck Millipore) at 1:200 in blocking solution for 1 h at RT. After three washes in PBS, cells were incubated for 1 h at RT with donkey anti-mouse secondary antibody conjugated with Alexa Fluor 488 (Invitrogen Life Technologies) at a 1:300 dilution. Nuclei were counterstained using Hoechst 33258 (Invitrogen Life Technologies) for 5 min and washed thrice with PBS. A small amount of PBS was left to keep surfaces wet hence to avoid monolayer drying. Samples were analyzed with an inverted fluorescent microscope (DM4000b, Leica) using GFP (for TUBβ3) and A4 (for nuclei) filters. TUBβ3 and nuclei images were overlapped using LAS AF lite software (Leica).

Statistical analysis

Statistical analysis was performed using paired Student's t-test, and results were considered significant when $p < 0.05$.

Results

Immunophenotypical characterization & multipotency features of hCMCs

We isolated multipotent stem cells from human peripheral blood samples and characterized their immunophenotypical, growth and differentiative properties. hCMCs adhere to plastic showing fibroblast-like morphology (Figure 1A). Cell homogeneity for the expression of CD44, CD73, CD105 and Nestin (known to characterize multidifferentiative stem cells populations) [19–21] is highlighted by flow cytometry (Figure 1B) in > 97% of short and long term cultures, suggesting that stemness properties are preserved under *in vitro* expansion. However, hCMCs are heterogeneous for CD34 (29.2 ± 2.5%), CD90 (76.0 ± 3.2%) and CD33 (11.5 ± 1.2%) [22–25]. A very strong reduction in the expression levels of CD34 (dropping down to 0%) and CD90 (down to 12.0 ± 2.8%) in long-term cultures is observed, according to negative modulation induced by *ex vivo* conditions on cell adhesive properties. Interestingly, the invariant expression of CD33, a member of the sialic acid-binding Ig-like lectin (Siglec) family, from short to long term culture suggests potential inhibitory activities of hCMCs during inflammation [23]. As expected, CD14, CD45 and HLA-DR (which are expressed by mature hematopoietic cells) [24], are not detected. When expanded for 40 *in vitro* passages, hCMCs show high self-renewal capacity, with 60 h doubling time (not shown). In addition, their high stemness grade is demonstrated by quantitative PCR (qPCR) evidence on the expression of pluripotency genes *NANOG*, *OCT4*, *REX1*, *SOX2*, *KLF4*, *CMYC*, *NOTCH* and *STAT3* (Figure 1C). When cultured under proper differentiative conditions, hCMCs show high plasticity toward adipocyte-, osteoblast-, myocyte-like phenotypes, as demonstrated by the expression of leptin, osteocalcin and tropomyosin 1 genes (Figure 1D).

hCMCs neuronal differentiation

Besides the commitment toward mesodermal lineages, we checked the neurogenic potential of hCMCs by culturing in DMEM/F-12 + 2% FBS added or not with 10 µM RA, for comparison to inductive conditions used with SH-SY5Y cells [9]. In parallel, samples grown in αMEM + 16.5% FBS (standard medium) were used as control for nonexogenously stimulated cells. DMEM/F-12 is a complex medium widely used for culturing neuronal cells [26,27] and inducing neuronal differentiation of neural precursors or stem cells when supplemented with either specific growth factors [28–30] or RA [31–33].

The three aforementioned media proved to support the cellular growth (Figure 2A & B); however, they differently conditioned the neuronal induction of hCMCs. The expression of *Nestin* (neuronal precursors marker gene) [34] remains stable in control cells while showing a decreased level in cultures maintained in DMEM/F-12 for five days (Figure 2C). At day 3, mRNA expression of *TUBß3* (encoding a microtubule element found almost exclusively in neurons) [35] is higher in cells grown in DMEM/F-12 than in control (Figure 2D). The expression of other neuronal markers – *MAP2* [36] and neuronal isoform of *L1 CAM* – does not significantly vary after 24 h in either stimulated or control cells, while increased levels are observed since third day in DMEM/F-12 (Figure 2E & F).

We found that the morphology of RA-treated hCMCs is even wider than untreated cells after 5 days in culture (Figure 2A) and RA does not improve neuronal markers expression in hCMCs (Figure 2C–F). This further prompted us to set up a self-standing differentiative system by omitting RA stimulation in all next experiments with DMEM/F-12 medium. Similarly to bone marrow stem cells [37], hCMCs cultured in αMEM express neurotrophic factors such as NGF and BDNF (Figure 2G, left panel). When stimulated with DMEM/F-12, hCMCs show meaningfully increased expression of NGF, BDNF and GDNF (Figure 2G, right panel).

CNT–PLLA scaffold effects on hCMCs growth & differentiation

We recently reported that CNT–PLLA scaffolds in which derivatized CNTs are dispersed at low concentrations in PLLA, keep the full biocompatibility of the polymer matrix while improving scaffold nanotopography and conductivity and thus overperform PLLA alone in boosting growth and differentiation of SH-SY5Y cells [9]. Therefore, we wondered if the electrical/topographical stimuli from the same scaffolds could also drive stem cell populations such as hCMCs to start neuronal differentiation. Twenty-four hours from seeding, cells show homogeneous spreading onto CNT–PLLA (Figure 3A). During the entire differentiation time, CNT–PLLA does not alter cell proliferation (Figure 3B), while influencing instead cell morphology. When compared with controls, hCMCs seeded onto the scaffold show typical features of cells from the neuronal lineage, such as more restricted cell bodies (Figure 3C) and polarized appearance (Figure 3D). Moreover, hCMCs grown onto CNT–PLLA show a significant increase in both total length and number

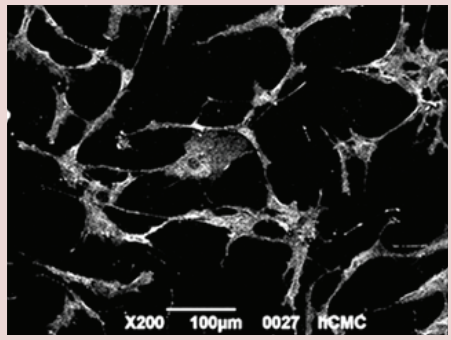

Antigens	Percentage of positive cells	
	Short-term cultures	Long-term cultures
CD33	11.5 ± 1.2	13.6 ± 1.4
CD34	29.2 ± 2.5	0.0 ± 0.0
CD44	98.9 ± 2.1	97.1 ± 1.7
CD73	99.3 ± 2.9	100.0 ± 1.9
CD90	76.0 ± 3.2	12.0 ± 2.8
CD105	100.0 ± 6.5	98.4 ± 2.7
Nestin	99.2 ± 3.1	97.2 ± 2.3
CD14	ND	ND
CD45	ND	ND
HLA-DR	ND	ND

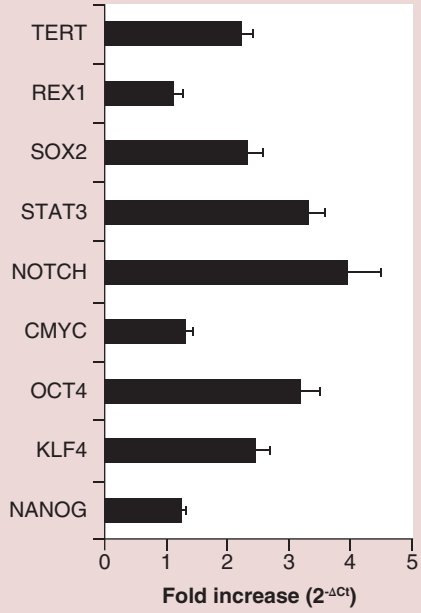

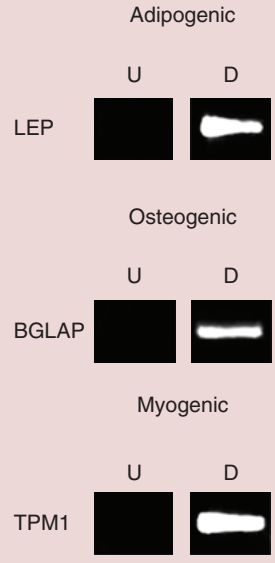

Figure 1. Morphological study and stemness characterization of human circulating multipotent cells. (A) Scanning electron microscopy image of human circulating multipotent cells seeded onto a glass coverslip; scale bars and magnification are reported in the picture; **(B)** Immunophenotypical characterization by FCM of short and long term cultures under standard conditions. Data are expressed as percentage (%) of positives ± standard deviation (SD) for each marker compared with isotype- or II Ab-matched control; ND; **(C)** mRNA expression of pluripotency markers by quantitative PCR on cells grown in standard medium. The comparative CT method ($2^{-\Delta Ct}$ ± SD) was used to quantify gene expression level. **(D)** Analysis of multidifferentiative potentialities by One Step RT-PCR Kit on human circulating multipotent cells cultured in standard (U) and specific induction medium (D) for 14 days. Amplified products were electrophoresed on 2% agarose gel and stained by GelRed™. *HPRT* was used as housekeeping gene.
ND: Not detected.

of protrusions per cell (Figure 3E & F), as well as neurite-like protrusions that are tipped with fan-shaped structures resembling growth cones (Figure 3G). Such a morphological response is confirmed by qPCR, as a sudden change in gene expression occurs soon after cell seeding onto the scaffolds. *Nestin* is strongly upregulated 24 h after seeding onto CNT–PLLA; then, its expression decreases during culturing, but it remains higher than control (Figure 3H). Compared to controls, a progressive upregulation of *MAP2* in cells growing onto the scaffolds becomes particularly evident since day 3 from seeding, while expression remains quite constant in control cells (Figure 3I). The expression of *TUBβ3* is highly upregulated soon after cell seeding onto the scaffolds and is significantly higher than control along the differentiation time (Figure 3L). At day 5, TUBβ3 protein is detected by immunofluorescence (Figure 3M) in approximately 77% of cells cultured

onto CNT–PLLA (Figure 3N) and approximately 23% of controls seeded on polystirene.

eCNT–PLLA scaffold effects on hCMCs growth & differentiation

For comparison to previous performance with SH-SY5Y cells [11], we used the same electrospun CNT–PLLA (eCNT–PLLA) scaffolds to provide hCMCs with sub-micrometric-sized fibers able to mimic the neuronal processes and the fibrillar collagenous and laminin component of the ECM. Cell proliferation is not impaired with respect to control when culturing hCMCs onto eCNT–PLLA scaffolds (Figure 4A), which show to drive cell morphological changes toward neuronal differentia-

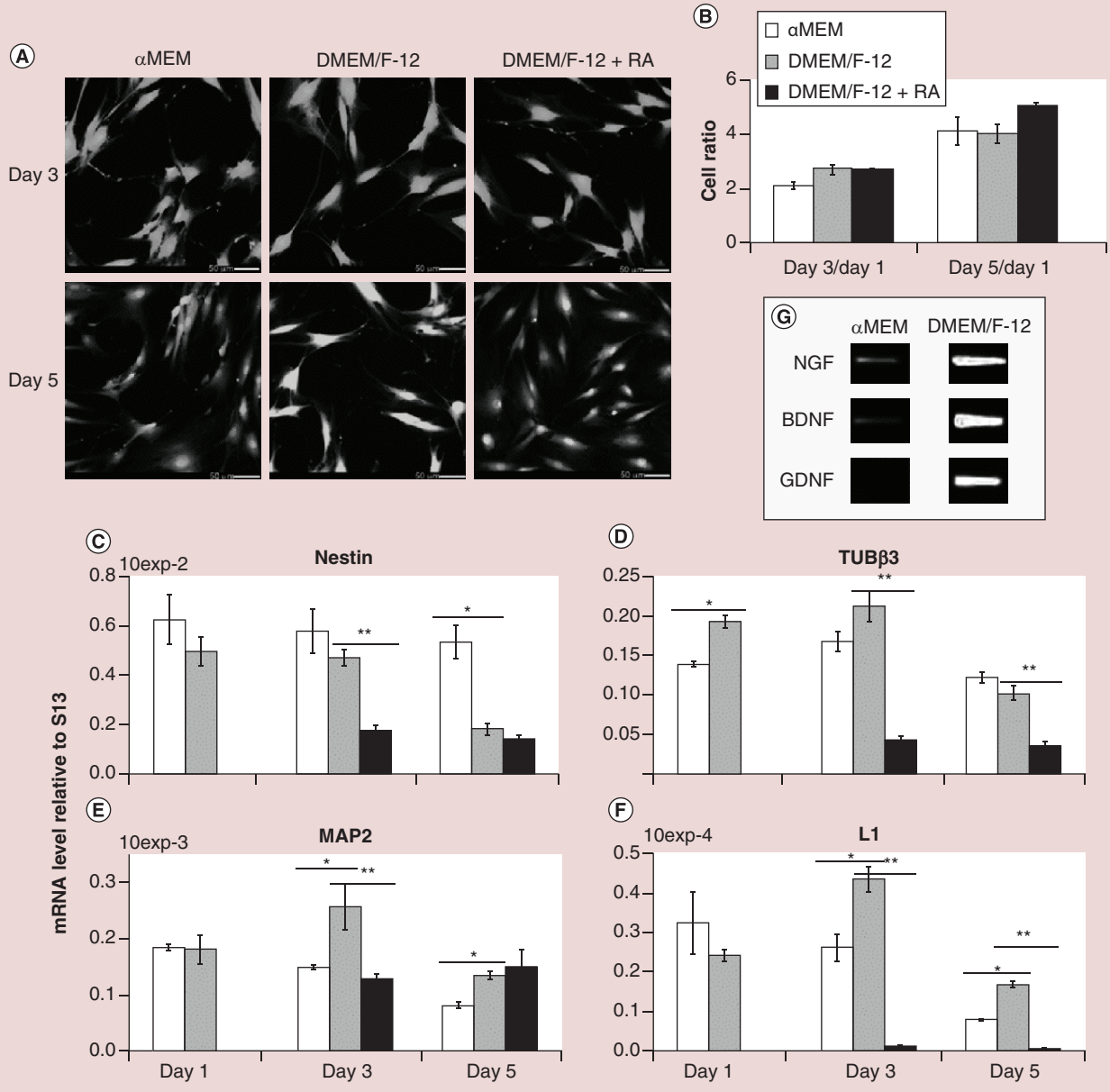

Figure 2. Growth and neuronal marker gene expression of human circulating multipotent cells in different culture media. (A) Human circulating multipotent cells (hCMCs) stained with Calcein-AM; image magnification is 20X. Scale bars are shown in the pictures. **(B)** hCMC proliferation in different media (color code is shown); data represent the mean ± standard error of the mean (M ± SEM) of three independent experiments performed in triplicate. **(C–F)** Expression profiles of **(C)** *Nestin*, **(D)** *TUBβ3*, **(E)** *MAP2* and **(F)** *L1 CAM* genes in hCMCs cultured in different media (same code as in B). **(G)** Analysis of neurotrophin expression by One Step RT-PCR Kit on hCMCs cultured in αMEM or DMEM/F-12 medium for 14 days.
*Shows significance at $p < 0.05$ between αMEM and DMEM/F-12 cultured samples.
**Shows significance at $p < 0.05$ between DMEM/F-12 and DMEM/F-12 + RA cultured samples.

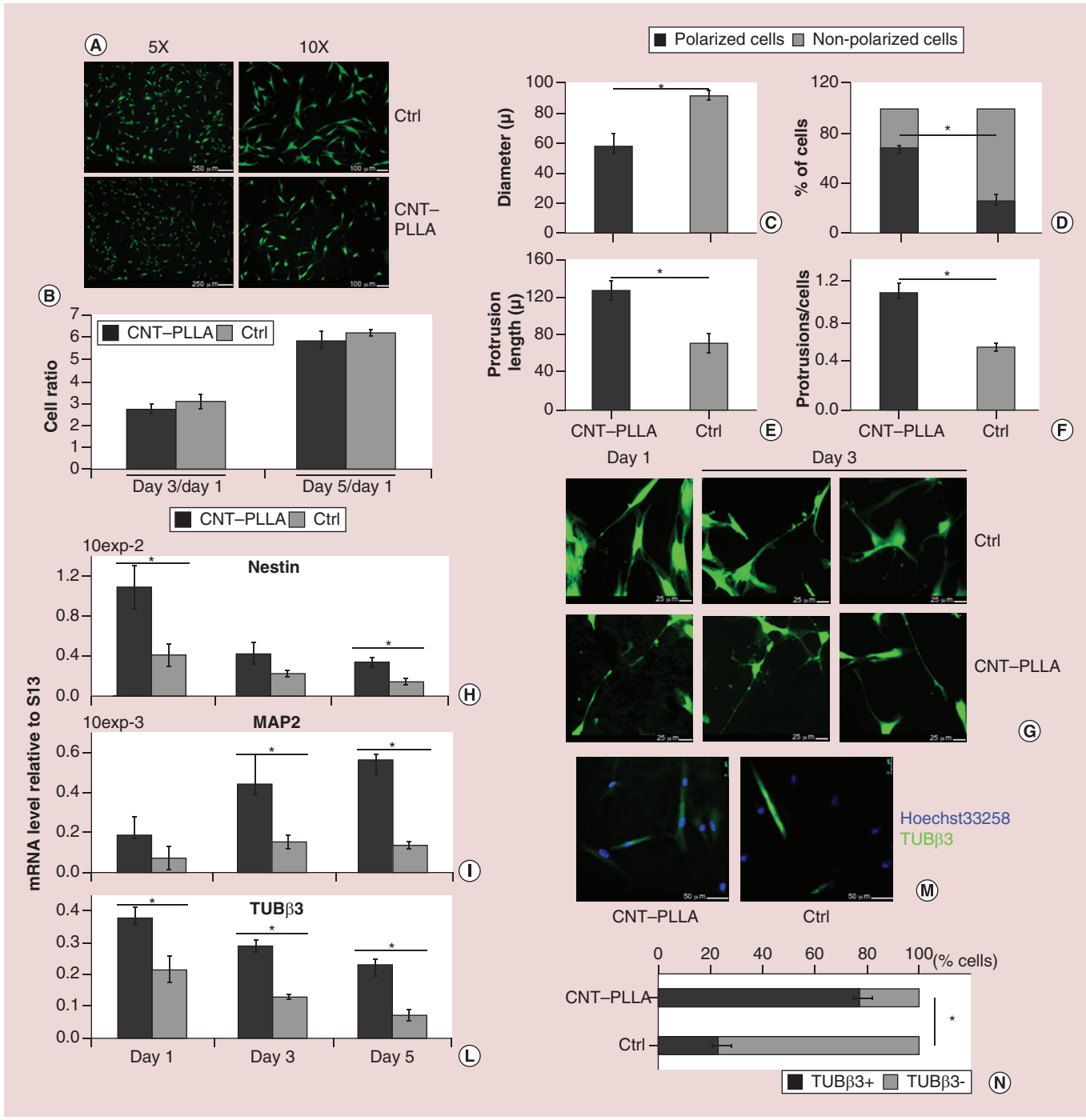

Figure 3. Effects of the CNT–PLLA scaffolds on human circulating multipotent cell growth and differentiation. **(A)** Human circulating multipotent cells (hCMCs) stained with Calcein-AM 24 h after seeding; image magnification is reported. **(B)** Cell proliferation. **(C)** Mean cell diameter. **(D)** Percentage of polarized cells. **(E)** Total protrusion length. **(F)** Number of protrusions per cell. Quantification was performed 24 h after cell seeding. **(G)** hCMCs stained with Calcein-AM; image magnification is 32X. **(H–L)** Expression profiles of **(H)** *Nestin*, **(I)** *MAP2* and **(L)** *TUBβ3* genes in hCMCs cultured onto either plates (control) or CNT–PLLA scaffolds. **(M)** Immunofluorescence for TUBβ3 (green) in hCMCs after 5 days in culture. Nuclei are counterstained with Hoechst 33258 (blue). Image magnification is 20X. **(N)** Quantification of TUBβ3 expression reported as the percentage of TUBβ3 positive cells in the total amount of cell counted. All histograms represent the mean ± standard error of the mean of at least three independent experiments performed in triplicate.
*Shows significance at $p < 0.05$ between cells seeded onto CNT–PLLA scaffolds and control (well bottoms).
Crtl: Control sample.

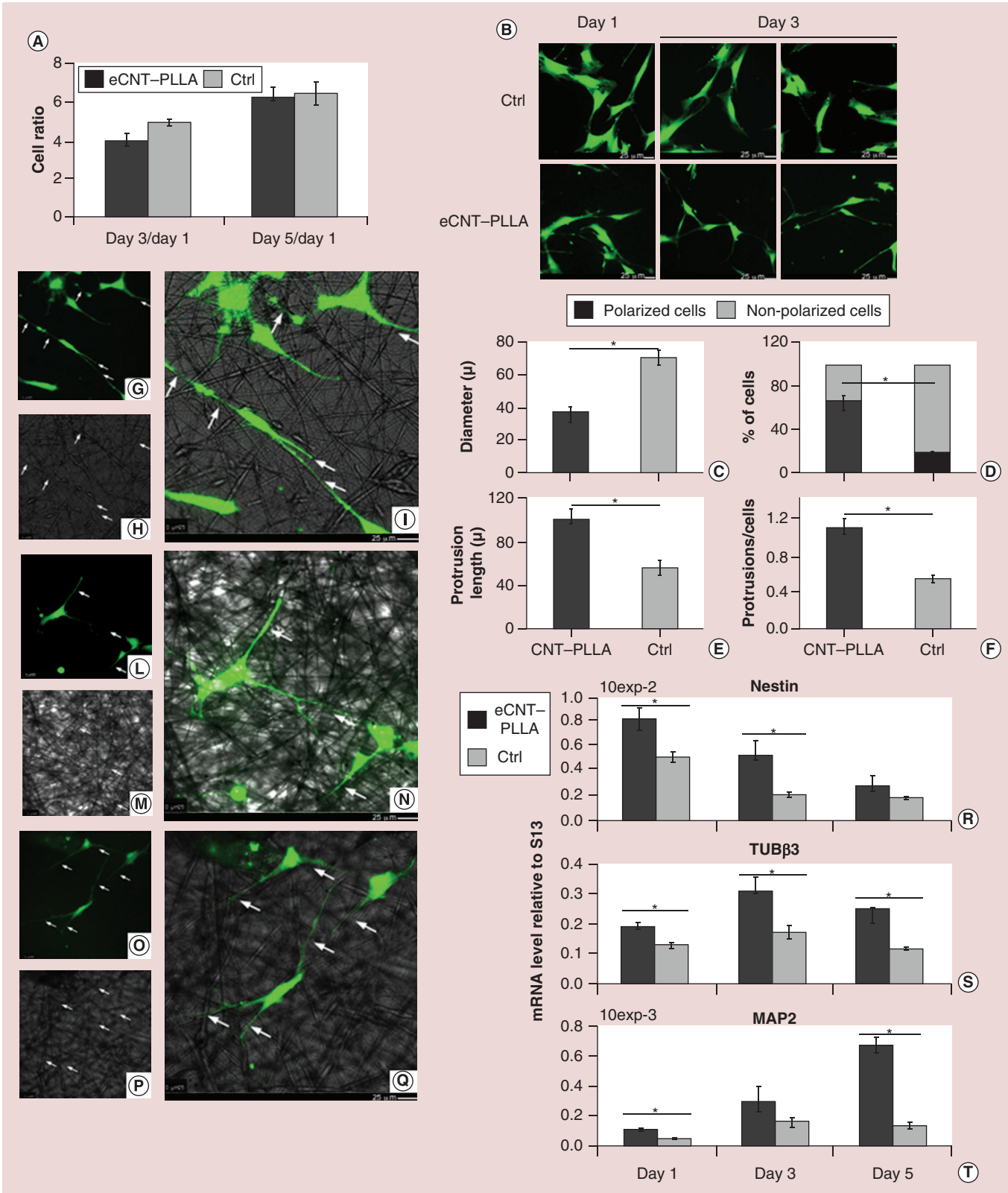

Figure 4. Effect of the eCNT–PLLA scaffolds on human circulating multipotent cell growth and differentiation. **(A)** Cell proliferation. **(B)** human circulating multipotent cells (hCMCs) stained with Calcein-AM; image magnification is 32X. **(C)** Mean cell diameter. *Shows significance at $p < 0.05$ between cells seeded on the eCNT–PLLA scaffolds and the control (well bottom). Ctrl: Control sample.

Figure 4. Effect of the eCNT–PLLA scaffolds on human circulating multipotent cell growth and differentiation (cont.). **(D)** Percentage of polarized cells. **(E)** Total protrusion length. **(F)** Number of protrusions per cell. Ctrl, control samples. Quantification was performed 24 h after cell seeding. **(G, L & O)** Fluorescent images of hCMCs stained with Calcein-AM. **(H, M & P)** bright field images of the eCNT–PLLA scaffolds. **(I, N & Q)** Superimpositions of cell fluorescent images and scaffold bright field images. White arrows indicate protrusions following the scaffold Fiber orientation. Image magnification is 32X. Expression profiles of **(R)** *Nestin*, **(S)** *TUBβ3* and **(T)** *MAP2* genes in hCMCs cultured onto either plates (Ctrl) or eCNT–PLLA scaffolds. All histograms represent the mean ± standard error of the mean of at least three independent experiments performed in triplicate.
*Shows significance at $p < 0.05$ between cells seeded on the eCNT–PLLA scaffolds and the control (well bottom).
Ctrl: Control sample.

tion (Figure 4B), such as, for example, diameter narrowing and fusiform shaping of the cell bodies (Figure 4C). Moreover, in comparison to control, hCMCs increasingly show a polarized appearance (Figure 4D) with longer and numerous neurite-like protrusions (Figure 4E & F). The superimposition of the Calcein-AM stained cells and the bright field images of the corresponding portion of the eCNT–PLLA scaffold, shows that hCMCs protrusions follow scaffold Fiber orientation (as highlighted by white arrows in Figure 4G–Q).

Quantitative gene expression analysis reveals a scaffold-dependent upregulation of some markers of the neuronal lineage. Indeed, a higher expression of *Nestin*, *TUBβ3* and *MAP2* is observed in cells grown onto eCNT–PLLA compared with controls (Figure 4R–T), hence suggesting that a neuronal differentiation program activation has started.

L1-A & LINGO1-A effects on hCMCs growth & differentiation

We recently developed and characterized biomimetic L1-A and LINGO1-A peptides, which proved to boost neuronal differentiation of SH-SY5Y cells [9]. Such peptides confirmed full biocompatibility, and neuritogenic properties when used on human stem cell cultures (Figure 5A). After treatment with peptides, hCMCs partly show (as expected in early differentiation stages) neuron-like morphology with small cell bodies and long protrusions resembling neurites (Figure 5B). qPCR evidence confirms that both peptides do influence the expression of both *Nestin* and *TUBβ3* genes, which are upregulated 24 h from the administration of L1-A and LINGO1-A (Figure 5C & D), while *MAP2* is upregulated only in cells treated with L1-A (Figure 5E).

Effects of the scaffold-peptides combination on neuronal growth & differentiation

Considered that both scaffolds (either electrospun or not) and peptides seem to commit hCMCs toward the neuronal lineage, we seeded hCMCs onto CNT scaffolds and treated them with L1-A and LINGO1-A to assess whether the combined effects of scaffolds and peptides could enhance the differentiation process. Cell proliferation is not influenced (Figure 6A), while qPCR analysis unveils a higher expression of *Nestin* during the entire progression of differentiation, compared with the cells either grown onto well bottoms or missing peptide treatment (Figure 6B). Over days 3 to 5 in culture, cells simultaneously treated with scaffold and peptides reveal an upregulation of *TUBβ3* (Figure 6C). Compared to controls, an increased expression of *MAP2* is observed (Figure 6D), largely at day 3 in hCMCs treated with L1-A onto CNT–PLLA scaffolds and at day 5 with LINGO1-A onto CNT–PLLA and eCNT–PLLA scaffolds. Specificity of the differentiative induction was further investigated evaluating the expression of other neuronal and non-neuronal genes. Interestingly, the endogenous expression of *L1 CAM* is improved by the scaffold + peptides combination, in particular by CNT–PLLA + LINGO1-A, while the expression is very low in cells growing onto the well bottoms (Figure 6E). As shown in Figure 6F, after 5 days in culture, the expression of *Syp* (a synaptic vesicle marker related to neuron maturation) [38] is much higher than that of three non-neuronal genes: *Runx2* (osteogenic marker) [39], *Myh7* (skeletal muscle marker) [40] and *Lep* (adipocyte marker) [41]; moreover, such non-neural markers show to be downregulated by the presence of the scaffolds and the peptides. Finally, *Syp* expression is upregulated in L1-A treated samples, regardless the presence of the scaffolds.

At day 5, FMC analysis of TUBβ3 protein level highlights that TUBβ3 expression is strictly controlled by cell–cell interactions, as well as by physical and soluble factors. Under standard culture conditions, TUBβ3 is not expressed in hCMCs (Figure 6G), while differentiating stimulation results in significantly increased expression levels; as reported in Figure 6H (middle panel), hCMCs cultured onto CNT–PLLA scaffolds and stimulated with L1-A or LINGO1-A show the highest values of mean fluorescence intensity. This evidence is consistent with qPCR data highlighting a combined/synergistic effect of electrical/nanotopographical stimuli (by the CNT–PLLA scaffolds) and molecular inducers (by the biomimetic peptides) on cell differentiation.

Discussion

Evidence reported in this work highlights that hCMCs – in addition to being a precious source of autologous stem cells that can be isolated from peripheral blood and propagated *in vitro* – respond well to differen-

tiative stimuli, including those ones eliciting neuronal differentiation. In fact, even a culture medium shift (from αMEM to DMEM/F-12) is able to favor the expression of markers of the neuronal lineage such as, for example, *TUBß3*, *MAP2* and neuronal *L1 CAM* [9,35,36]. hCMCs resemble immunophenotypical and differentiative properties of mesenchymal stem cells and mesoangioblasts; therefore, evidence that these cells express *Nestin per se* is not surprising, as *Nestin* is expressed in both neural progenitor cells [34] and endothelial precursors [42]. This suggests that hCMCs are suitable for nerve injury treatment. Morphological evidence further highlights that when growing onto CNT-polymer scaffolds, hCMCs are committed toward the neuronal lineage and show typical features of neuronal differentiation, such as reduced size of cell bodies, polarized appearance and presence of neurite-like protrusions. Moreover, such protrusions (which align to fibers, when growing onto eCNT–PLLA, confirming observations with SH-SY5Y cells [11]) are tipped with fan-shaped structures resembling growth cones. Concerning qPCR evidence, hCMCs seeded onto the CNT-polymer scaffolds show an early upregulation of *Nestin*, indicating that cells are undertaking the differentiation pathway toward neural progenitor cells like neurons, oligodendrocytes and astrocytes. Concomitant upregulation of *TUBβ3*, specific to immature and post-mitotic neurons [35], confirms that the majority of cells are acquiring a neuron-specific commitment. *MAP2* expression is upregulated as well in CNT-polymer samples and it progressively increases until day 5 of differentiation. Indeed, it is known that the expression of *MAP2* is temporally shifted with respect to neuron-specific *TUBβ3* as, during neurite initiation, *MAP2* is later involved in the coordinated reorganization of cytoskeleton networks of microtubules and filamentous actin [36].

Considering the robust literature on CNT-based nanocomposites and based on our knowledge of the hCMC cells, it is tempting to speculate that improved differentiation of hCMCs is likely favored by a number of intrinsic scaffold features: the nanoroughness of CNT nanocomposite scaffolds is known to match the size of the finest neuronal processes, favoring cell adhesion, neurite extension and differentiation toward the neuronal lineage by mimicking the neural environment topography [43]; hCMCs produce neurotrophins, such as NGF and GDNF, which play a well known role in the control of cell proliferation and differentiation; such factors are likely to bind to the scaffolds – thanks to the peculiar chemical properties of the used CNT–PLLA scaffolds [9,11] and the enhanced surface area of this kind of nanocomposites [13,43] – hence acting as a reservoir for self-eliciting growth and differentiation;

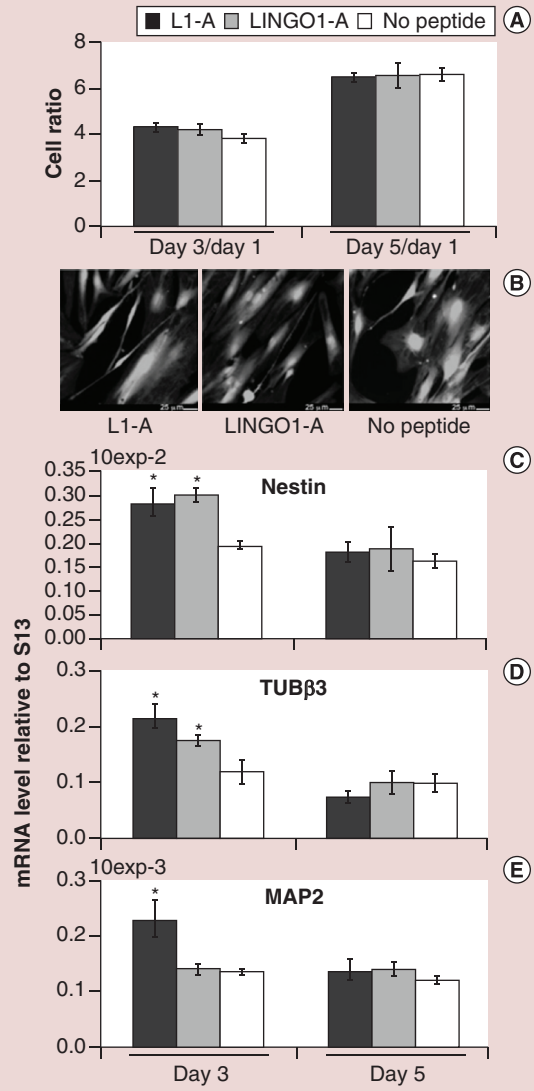

Figure 5. Effects of the biomimetic peptides on human circulating multipotent cell growth and differentiation. **(A)** Cell proliferation. **(B)** Human circulating multipotent cells stained with calcein-AM, 24 h after peptide administration; image magnification is 32X. Expression profiles of **(C)** *Nestin*, **(D)** *TUBβ3* and **(E)** *MAP2* genes in human circulating multipotent cells in the absence or presence of either L1-A or LINGO1-A biomimetic peptides. All histograms represent the mean ± standard error of the mean of at least three independent experiments performed in triplicate. *Shows significance at $p < 0.05$ between peptide treated samples and the control.

CNTs proved to enhance scaffold conductivity [9,11,15], which assists stem cell neuronal differentiation in the absence of external stimulation [6,44–46].

Moreover, modulating cell shape plays a central role in directing the fate of differentiation, because it can influence nucleus shape affecting in turn nuclear matrix proteins and focal adhesion complexes and thus

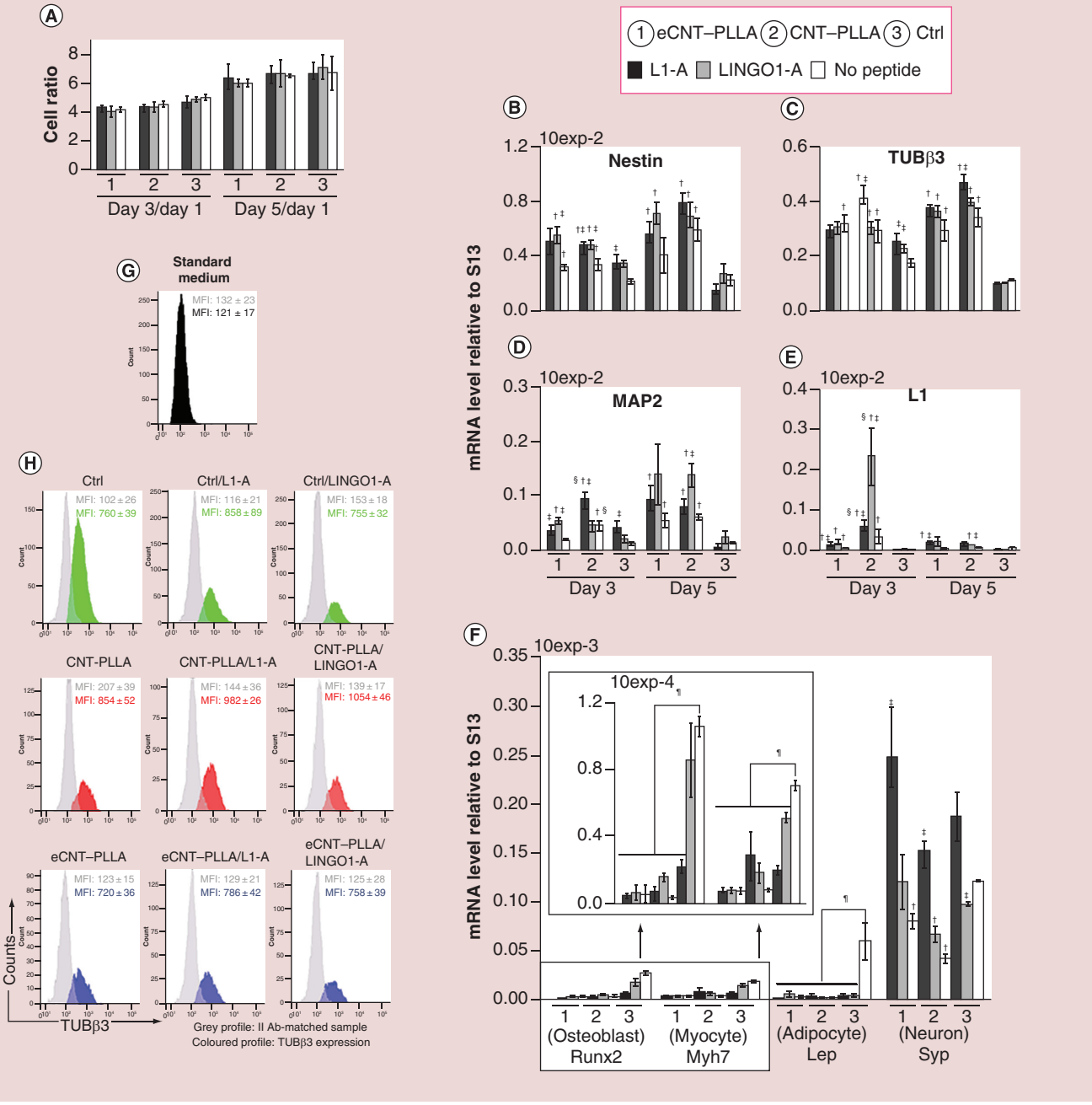

Figure 6. Combined effect by nanocomposite scaffolds and biomimetic peptides on human circulating multipotent cell growth and differentiation. A unique color and numbering code for all panels is shown in the red box. **(A)** Cell proliferation. Expression profiles of **(B)** *Nestin*, **(C)** *TUBβ3*, **(D)** *MAP2*, **(E)** *L1 CAM* and **(F)** *Runx*, *Myh7*, *Lep* and *Syp* genes in human circulating multipotent cells (hCMCs) cultured onto either plates (control) or the nanocomposite scaffolds and treated by L1-A, LINGO1-A or no peptide. As shown by the arrows, the upper-left inset in **(F)** represents a magnification of *Runx* and *Myh7* expression data. Data represent the mean ± SEM of at least three independent experiments performed in triplicate. FCM analysis of TUBβ3 expression in **(G)** standard cultures (αMEM medium) and **(H)** DMEM/F-12 cultures (scaffold and/or peptide treatment). **(H)** Grey profiles concern secondary antibody-matched samples and colored ones indicate TUBβ3 expression. Data are expressed as mean fluorescence intensity ± SD of three independent experiments performed in triplicate.

†Shows significance at $p < 0.05$ between samples grown onto the scaffolds and control (well bottom).

‡Shows significance at $p < 0.05$ between peptide-treated and untreated samples (same substrates).

§Shows significance at $p < 0.05$ between samples grown onto CNT–PLLA and eCNT–PLLA scaffolds (same peptide treatment).

¶Shows significance at $p < 0.05$ between control cells (well bottoms, no peptide treatment) and treated samples (seeded onto the scaffolds and/or treated with peptides).

Ctrl: Control sample.

the expression of silent genes [47]. Intriguingly, when growing onto our scaffolds, hCMCs show polarized cell shape and reduced cell body size.

The combination of CNT-based scaffolds with growth factors and/or animal derived matrices can modulate embryonic, mesenchymal and neural stem cell commitment toward neurogenesis *in vitro* [43,47–51]. Moving one step ahead, this study reports on CNT-based scaffolds able to promote *per se* stem cell differentiation toward the neuronal lineage, while ensuring at the same time full implantability for *in vivo* applications, as the synthetic PLLA polymer is 100% biocompatible and free from immunogenicity issues [52] with animal-derived materials, including collagen [53]; moreover the high dispersion of CNTs in the PLLA matrix keeps full biocompatibility [9] and makes the scaffold self-standing and flexibile, in other words, suitable for properly shaping and well fitting into the injured site. Thanks to the fibrous morphology of the eCNT–PLLA scaffold, with fibers diameters partially overlapping the diameter range of both axons (80 nm–20 µm) and collagen fibrils (260–410 nm) [11] and to the presence of CNTs creating a nanotexture that can provide sites for cellular anchorage and guidance of cytoskeletal extension, we found that the eCNT–PLLA scaffolds not only commit hCMCs toward neuronal lineage, but they also guide protrusion extensions that indeed follow the scaffold fiber orientation.

To the best of our knowledge, this study represents the first report on human adult stem cells derived from blood to be cultured onto CNT-based scaffolds, and to be induced toward neuronal differentiation even in the absence of exogenously added, classic neurotrophins or other inducers, in other words, only by the scaffold capacity to mimic tissue relevant nanotopographical features. In addition to being a precious source of stem cells exploitable for such an applications, hCMCs present some advantages in comparison to other stem cells: they are neither subjected to ethical restrictions nor genetically transformed; moreover, hCMCs can be isolated in larger amounts than neural stem cells (NSCs) and more easily isolated and in a less invasive way than both NSCs (brain) [54] and MSCs (mainly bone marrow) [55]. Since the developed tissue-mimetic system supports cell growth onto a biocompatible environment that contains instructions able to boost neuronal differentiation, scaffolds could be transplanted to neuron-injured sites to promote and support hCMCs differentiation without the addition of soluble factors that are difficult to administrate and pattern *in vivo* [13].

Evidence from morphological observation and neuronal marker expression that biomimetic peptides can influence hCMCs differentiation without altering cell proliferation is in agreement with the fact that they are derived from homo-/heterophilic binding motifs of CAM/ECM proteins exposed at the neuronal surface and involved in regulation of neurite outgrowth, guidance and neuronal differentiation [9]. Indeed, morphology of peptide-treated cells is sharper than that of control cells; moreover, the two peptides induce the formation of long protrusions resembling neurites, and stimulate the expression of neuronal cytoskeleton markers, such as Nestin, TUBβ3 and MAP2 that play an important role in neuronal architecture definition [34–36]. Therefore, culture conditions are likely to stimulate the expression of peptide target molecules and then, after peptide administration, neuronal differentiation is further promoted.

When hCMCs are simultaneously seeded onto nanocomposite scaffolds and treated with peptides, neuronal differentiation is further promoted and, in most cases, *Nestin*, *TUBß3*, *MAP2* and *L1 CAM* genes show the highest expression values. The specificity of neuronal commitment seems to be further confirmed by downregulation of non-neuronal marker expression depending on peptide treatment and/or cultivation onto the scaffolds.

Conclusion

Aforementioned results suggest that our nanocomposite scaffolds are able to initiate hCMCs neuronal differentiation through the expression of neuronal specific markers; then, the peptide administration further promotes hCMCs neuronal commitment as peptides are likely to encounter their specific binding partners on cell surfaces thanks to the initial neuronal induction exerted by the scaffolds. Such synergistic effect in promoting hCMCs neuronal commitment confirms evidence with neuroblast-like precursors [9,11] and suggests the idea to covalently functionalize the scaffolds with peptides – more stable and less immunogenic than entire proteins [56] – to enrich the spectrum of differentiating cues able to more finely regulate cell differentiation and their spatial organization.

Future perspective

Further improvements in scaffold geometry and composition, functionalization with peptides and in culture conditions are needed to achieve a more complete neuronal differentiation of cells and to fine tune neuron subtype obtained. Nevertheless, our system moved a step forward in setting up implantable scaffolds suitable for autologous neuronal differentiation, especially thanks to the high plasticity of the cellular system. Electrospun nanofibrous scaffolds are becoming an elective material for tissue engineering [57–59] and indeed eCNT–PLLA capacity to 'drive' neuronal differentiation [11] might be further improved by

using aligned and peptide-derivatized eCNT–PLLA fibrous scaffolds consisting of topomimetic and biomimetic 'tracks' for process guidance. Future functional assessment of synaptic transmission and electrophysiological properties of cells onto the scaffolds will be of great interest. Moreover, coupling such scaffolds with electrical stimulation (which is readily achievable using CNT based materials) can boost further analyses aimed at studying neuronal differentiation and have great potential in nerve injury repair as well as neuron prosthesis.

Financial & competing interests disclosure

The authors acknowledge the financial support from CaRiPaRo Foundation (Excellence Research Project 2011 to V De Filippis), the Italian Ministry of Education, Universities and Research – MIUR (contract PRIN-20104XET32 to E Menna) and the University of Padova, Italy (basic "EX 60%" grants to R Di Liddo and F Filippini, Project PRAT2015 CPDA151948 to F Filippini). Research fellowship CPDR137224/13 to R Di Liddo (supporting T Bertalot) and PhD fellowship to G Scapin are gratefully acknowledged. The authors have no other relevant affiliations or financial involvement with any organization or entity with a financial interest in or financial conflict with the subject matter or materials discussed in the manuscript apart from those disclosed.

No writing assistance was utilized in the production of this manuscript.

Ethical conduct of research

The authors state that they have obtained appropriate institutional review board approval or have followed the principles outlined in the Declaration of Helsinki for all human or animal experimental investigations. In addition, for investigations involving human subjects, informed consent has been obtained from the participants involved.

Executive summary

- Human circulating multipotent cells (hCMCs) represent an autologous source of cells that can be isolated from peripheral blood and show high degree of stemness and multidifferentiative potential.
- hCMCs present some advantages in comparison to other stem cells: they are neither subjected to ethical restrictions nor genetically transformed; moreover, hCMCs can be isolated in larger amounts than NSCs and more easily isolated and in a less invasive way than both NSCs (brain) and MSCs (mainly bone marrow).
- Nanocomposite scaffold consisting of a poly-L-lactic acid (PLLA) matrix and highly dispersed, functionalized carbon nanotubes (CNTs), keeps the full biocompatibility of PLLA with the electric and nanotopographical features of CNTs, thus properly mimicking the neural tissue environment.
- Both CNT–PLLA and eCNT–PLLA scaffolds are able to induce and drive differentiation of hCMCs toward neuronal lineage in the absence of exogenously added growth factors.
- The biomimetic peptides can further boost hCMC neuronal differentiation.
- The developed system is suggested as a prototype of freestanding scaffold and autologous cell source for neural regenerative medicine applications.

References

Papers of special note have been highlighted as:
• of interest; •• of considerable interest

1 Stenderup K, Justesen J, Clausen C, Kassem M. Aging is associated with decreased maximal life span and accelerated senescence of bone marrow stromal cells. *Bone* 33(6), 919–926 (2003).

2 Rubinstein P, Rosenfield RE, Adamson JW, Stevens CE. Stored placental blood for unrelated bone marrow reconstitution. *Blood* 81, 1679–1690 (1993).

3 Zuk PA, Zhu M, Ashjian P, De Ugarte DA, Huang JI, Mizuno H. Human adipose tissue is a source of multipotent stem cells. *Mol. Biol. Cell* 13, 4279–4295 (2002).

4 Seta N, Kuwana M. Human circulating monocytes as multipotential progenitors. *Keio J. Med.* 56(2), 41–47 (2007).

• **This paper reports on the presence of multipotent cells in the circulating blood niche.**

5 Pettikiriarachchi JTS, Parish CL, Shoichet MS, Forsythe JS, Nisbet DR. Biomaterials for brain tissue engineering. *Aust. J. Chem.* 63, 1143–1154 (2010).

6 Fabbro A, Prato M, Ballerini L. Carbon nanotubes in neuroregeneration and repair. *Adv. Drug Deliv. Rev.* 65(15), 2034–2044 (2013).

7 Kotov AN, Winter JO, Clements IP *et al.* Nanomaterials for neural interfaces. *Adv. Mater.* 21, 3970–4004 (2009).

8 Lovat V, Pantarotto D, Lagostena L *et al.* Carbon nanotube substrates boost neuronal electrical signaling. *Nano Lett.* 5(6), 1107–1110 (2005).

9 Scapin G, Salice P, Tescari S, Menna E, De Filippis V, Filippini F. Enhanced neuronal cell differentiation combining biomimetic peptides and a carbon nanotube-polymer scaffold. *Nanomedicine* 11(3), 621–632 (2015).

•• **This work reports on the set up and characterization of nanocomposite carbon nanotube (CNT)–poly-L-lactic acid scaffolds and biomimetic peptides as a tool to boost neuronal differentiation of human neuroblastoma derived SH-SY5Y cells. These scaffolds and peptides are then used in this work.**

10 Lopes FM, Schröder R, da Frota ML Jr *et al.* Comparison between proliferative and neuron-like SH-SY5Y cells as an

in vitro model for Parkinson disease studies. *Brain Res.* 1337, 85–94 (2010).

11 Vicentini N, Gatti T, Salice P *et al.* Covalent functionalization enables good dispersion and anisotropic orientation of multi-walled carbon nanotubes in a poly(L-lactic acid) electrospun nanofibrous matrix boosting neuronal differentiation. *Carbon* 95(12), 725–730 (2015).

•• **In this work, scaffolds like those set up in reference 9 are electrospun to produce nanofibers driving neuronal processess of SH-SY5Y cells. These scaffolds are then used in this work.**

12 Bareket-Keren L, Hanein Y. Carbon nanotube-based multielectrode arrays for neuronal interfacing: progress and prospects. *Front. Neural Circuits* 6, 122 (2013).

13 Chen YS, Hsiue GH. Directing neural differentiation of mesenchymal stem cells by carboxylated multiwalled carbon nanotubes. *Biomaterials* 34(21), 4936–4944 (2013).

14 Landers J, Turner JT, Heden G *et al.* Carbon nanotube composites as multifunctional substrates for *in situ* actuation of differentiation of human neural stem cells. *Adv. Health Mater.* 3(11), 1745–1752 (2014).

• **This work together with reference 15, highlights CNT-based nanocomposites as elective material for neuronal differentiation.**

15 Lizundia E, Sarasua JR, D'Angelo F *et al.* Biocompatible poly(L-lactide)/MWCNT nanocomposites: morphological characterization, electrical properties, and stem cell interaction. *Macromol. Biosci.* 12(7), 870–881 (2012).

• **This work together with reference 14, highlights CNT-based nanocomposites as elective material for neuronal differentiation.**

16 Di Liddo R, Bertalot T, Schuster A *et al.* Anti-inflammatory activity of Wnt signaling in enteric nervous system: *in vitro* preliminary evidences in rat primary cultures. *J. Neuroinflammation* 12, 23 (2015).

17 Vacca M, Albania L, Della Ragione F *et al.* Alternative splicing of the human gene SYBL1 modulates protein domain architecture of Longin VAMP7/TI-VAMP, showing both non-SNARE and synaptobrevin-like isoforms. *BMC Mol. Biol.* 12, 26 (2011).

18 Huang YA, Kao JW, Tseng DT, Chen WS, Chiang MH, Hwang E. Microtubule-associated type II protein kinase A is important for neurite elongation. *PLoS ONE* 8(8), e73890 (2013).

19 Kolf CM, Cho E, Tuan RS. Mesenchymal stromal cells. Biology of adult mesenchymal stem cells: regulation of niche, self-renewal and differentiation. *Arthritis Res. Ther.* 9(1), 204 (2007).

20 He Q, Wan C, Li G. Concise review: multipotent mesenchymal stromal cells in blood. *Stem Cells* 25(1), 69–77 (2007).

21 Méndez-Ferrer S, Michurina TV, Ferraro F *et al.* Mesenchymal and haematopoietic stem cells form a unique bone marrow niche. *Nature* 466(7308), 829–834 (2010).

22 Minasi MG, Riminucci M, De Angelis L *et al.* The meso-angioblast: a multipotent, self-renewing cell that originates from the dorsal aorta and differentiates into most mesodermal tissues. *Development* 129(11), 2773–2783 (2002).

23 Lajaunias F, Dayer JM, Chizzolini C. Constitutive repressor activity of CD33 on human monocytes requires sialic acid recognition and phosphoinositide 3-kinase-mediated intracellular signaling. *Eur. J. Immunol.* 35(1), 243–251 (2005).

24 Meregalli M, Farini A, Torrente Y. Mesenchymal stem cells as muscle reservoir. *J. Stem Cell Res. Ther.* 1, 105 (2011).

25 Li S, Huang KJ, Wu JC *et al.* Peripheral blood-derived mesenchymal stem cells: candidate cells responsible for healing critical-sized calvarial bone defects. *Stem Cells Transl. Med.* 4(4), 359–368 (2015).

26 Mahoney SA, Hosking R, Farrant S *et al.* The second galanin receptor GalR2 plays a key role in neurite outgrowth from adult sensory neurons. *J. Neurosci.* 23(2), 416–421 (2003).

27 Wang S, Ghezzi CE, White JD, Kaplan DL. Coculture of dorsal root ganglion neurons and differentiated human corneal stromal stem cells on silk-based scaffolds. *J. Biomed. Mater. Res. A* 103(10), 3339–3348 (2015).

28 Prabhakaran MP, Venugopal JR, Ramakrishna S. Mesenchymal stem cell differentiation to neuronal cells on electrospun nanofibrous substrates for nerve tissue engineering. *Biomaterials* 30(28), 4996–5003 (2009).

• **This manuscript highlights the added value of electrospun substrates for nerve tissue engineering.**

29 Zhang XQ, Zhang SC. Differentiation of neural precursors and dopaminergici neurons from human embryonic stem cells. *Methods Mol. Biol.* 584, 355–366 (2010).

30 Li YC, Tsai LK, Wang JH, Young TH. A neural stem/precursor cell monolayer for neural tissue engineering. *Biomaterials* 35(4), 1192–1204 (2014).

31 Påhlman S, Ruusala AI, Abrahamsson L, Mattsson ME, Esscher T. Retinoic acid-induced differentiation of cultured human neuroblastoma cells: a comparison with phorbolester-induced differentiation. *Cell Differ.* 14(2), 135–144 (1984).

32 Cañón E, Cosgaya JM, Scsucova S, Aranda A. Rapid effects of retinoic acid on CREB and ERK phosphorylation in neuronal cells. *Mol. Biol. Cell* 15(12), 5583–5592 (2004).

33 Rochette-Egly C. Retinoic acid signaling and mouse embryonic stem cell differentiation: cross talk between genomic and non-genomic effects of RA. *Biochim. Biophys. Acta* 1851(1), 66–75 (2015).

34 Dahlstrand J, Lardelli M, Lendahl U. Nestin mRNA expression correlates with the central nervous system progenitor cell state in many, but not all, regions of developing central nervous system. *Brain Res. Dev. Brain Res.* 84(1), 109–129 (1995).

35 Tischfield MA, Baris HN, Wu C *et al.* Human TUBB3 mutations perturb microtubule dynamics, kinesin interactions, and axon guidance. *Cell* 140(1), 74–87 (2010).

36 Dehmelt L, Halpain S. The MAP2/Tau family of microtubule-associated proteins. *Genome Biol.* 6(1), 204 (2005).

37 Crigler L, Robey RC, Asawachaicharn A, Gaupp D, Phinney DG. Human mesenchymal stem cell subpopulations express a variety of neuro-regulatory molecules and promote

neuronal cell survival and neuritogenesis. *Exp. Neurol.* 198(1), 54–64 (2006).

38 Harrill JA, Chen H, Streifel KM, Yang D, Mundy WR, Lein PJ. Ontogeny of biochemical, morphological and functional parameters of synaptogenesis in primary cultures of rat hippocampal and cortical neurons. *Mol. Brain* 8, 10 (2015).

39 De Coppi P, Bartsch G Jr, Siddiqui MM *et al.* Isolation of amniotic stem cell lines with potential for therapy. *Nat. Biotechnol.* 25(1), 100–106 (2007).

40 Wang M, Yu H, Kim YS, Bidwell CA, Kuang S. Myostatin facilitates slow and inhibits fast myosin heavy chain expression during myogenic differentiation. *Biochem. Biophys. Res. Commun.* 426(1), 83–88 (2012).

41 Taura D, Noguchi M, Sone M *et al.* Adipogenic differentiation of human induced pluripotent stem cells: comparison with that of human embryonic stem cells. *FEBS Lett.* 583(6), 1029–1033 (2009).

42 Mokrý J, Čížková D, Filip S *et al.* Nestin expression by newly formed human blood vessels. *Stem Cells Dev.* 13(6), 658–664 (2004).

43 Chao TI, Xiang S, Lipstate JF, Wang C, Lu J. Poly(methacrylic acid)-grafted carbon nanotube scaffolds enhance differentiation of hESCs into neuronal cells. *Adv. Mater.* 22(32), 3542–3547 (2010).

44 Ostrakhovitch EA, Byers JC, O'Neil KD, Semenikhin OA. Directed differentiation of embryonic P19 cells and neural stem cells into neural lineage on conducting PEDOT-PEG and ITO glass substrates. *Arch. Biochem. Biophys.* 528(1), 21–31 (2012).

45 Yamada M, Tanemura K, Okada S *et al.* Electrical stimulation modulates fate determination of differentiating embryonic stem cells. *Stem Cells* 25(3), 562–570 (2007).

46 Gordon T, Udina E, Verge VM, de Chaves EI. Brief electrical stimulation accelerates axon regeneration in the peripheral nervous system and promotes sensory axon regeneration in the central nervous system. *Motor Control* 13(4), 412–441 (2009).

47 Kim JA, Jang EY, Kang TJ *et al.* Regulation of morphogenesis and neural differentiation of human mesenchymal stem cells using carbon nanotube sheets. *Integr. Biol. (Camb.)* 4(6), 587–594 (2012).

48 Jan E, Kotov NA. Successful differentiation of mouse neural stem cells on layer-by-layer assembled single-walled carbon nanotube composite. *Nano Lett.* 7(5), 1123–1128 (2007).

49 Chen CS, Soni S, Le C *et al.* Human stem cell neuronal differentiation on silk-carbon nanotube composite. *Nanoscale Res. Lett.* 7(1), 126 (2012).

50 Tay CY, Gu H, Leong WS *et al.* Cellular behavior of human mesenchymal stem cells cultured on single-walled carbon nanotube film. *Carbon* 48(4), 1095–1104 (2010).

51 Lee JH, Lee JY, Yang SH, Lee EJ, Kim HW. Carbon nanotube-collagen three-dimensional culture of mesenchymal stem cells promotes expression of neural phenotypes and secretion of neurotrophic factors. *Acta Biomater.* 10(10), 4425–4436 (2014).

52 Yao F, Bai Y, Zhou Y, Liu C, Wang H, Yao K. Synthesis and characterization of multiblock copolymers based on L-lactic acid, citric acid, and poly(ethylene glycol). *J. Polym. Sci. A Polym. Chem.* 41(13), 2073–2081 (2003).

53 Boeer U, Buettner FF, Klingenberg M *et al.* Immunogenicity of intensively decellularized equine carotid arteries is conferred by the extracellular matrix protein collagen type VI. *PLoS ONE* 9(8), e105964 (2014).

54 Rietze RL, Reynolds BA. Neural stem cell isolation and characterization. *Methods Enzymol.* 419, 3–23 (2006).

55 Augello A, De Bari C. The regulation of differentiation in mesenchymal stem cells. *Hum. Gene Ther.* 21(10), 1226–1238 (2010).

56 Chen H, Yuan L, Song W, Wu Z, Li D. Biocompatible polymer materials: role of protein-surface interactions. *Prog. Polym. Sci.* 33, 1059–1087 (2008).

57 Ingavle GC, Leach JK. Advancements in electrospinning of polymeric nanofibrous scaffolds for tissue engineering. *Tissue Eng. Part B Rev.* 20(4), 277–293 (2014).

58 Biggs M, Pandit A, Zeugolis DI. 2D imprinted substrates and 3D electrospun scaffolds revolutionize biomedicine. *Nanomedicine (Lond).* 11(9), 989–992 (2016).

59 Ott LM, Zabel TA, Walker NK *et al.* Mechanical evaluation of gradient electrospun scaffolds with 3D printed ring reinforcements for tracheal defect repair. *Biomed. Mater.* 11(2), 025020 (2016).